CrossMark

ORIGINAL ARTICLE

Absorption of calcium ions on oxidized graphene sheets and study its dynamic behavior by kinetic and isothermal models

Mahmoud Fathy[1] · Th. Abdel Moghny[1] · Mahmoud Ahmed Mousa[2] ·
Abdel-Hameed A-A. El-Bellihi[2] · Ahmed E. Awadallah[3]

Abstract Sorption of calcium ion from the hard underground water using novel oxidized graphene (GO) sheets was studied in this paper. Physicochemical properties and microstructure of graphene sheets were investigated using Raman spectrometer, thermogravimetry analyzer, transmission electron microscope, scanning electron microscope. The kinetics adsorption of calcium on graphene oxide sheets was examined using Lagergren first and second orders. The results show that the Lagergren second-order was the best-fit model that suggests the conception process of calcium ion adsorption on the Go sheets. For isothermal studies, the Langmuir and Freundlich isotherm models were used at temperatures ranging between 283 and 313 K. Thermodynamic parameters resolved at 283, 298 and 313 K indicating that the GO adsorption was exothermic spontaneous process. Finally, the graphene sheets show high partiality toward calcium particles and it will be useful in softening and treatment of hard water.

Keywords Graphene · Graphene sheets · Adsorption · Isothermal · Kinetic · Thermodynamics parameters · Models

✉ Mahmoud Fathy
  fathy8753@yahoo.com

1   Applications Department, Egyptian Petroleum Research
    Institute (EPRI), 1 Ahmed El-Zomer, Nasr City,
    Box. No. 11727, Cairo, Egypt

2   Faculty of Science, Benha University, Fred Nada Street,
    Banha, Cairo, Egypt

3   Development of Processes Department, Egyptian Petroleum
    Research Institute, 1 Ahmed El-Zomer, Nasr City,
    Box. No. 11727, Cairo, Egypt

Introduction

For a long time, graphene was a simple idea used as a spellbinding method for more unpredictable types of fresh-smelling carbon and a basic framework for strong state theoreticians. Graphene is a nuclear scale where flimsy sheets of the cross section that made of carbon particles (Lin et al. 2013). The seclusion of a single or few layer graphene from graphite sources has pulled in expanding consideration because, knowing about graphene will display novel physical-concoction properties, like high values of Yong's modulus, crack quality (Wang et al. 2015a, b), warm conductivity, particular surface zone, adsorption limit, and electrical conductivity. Graphene nanosheets have pulled in impressive interest because of their curious properties in crucial research and potential mechanical applications in vitality stockpiling materials (Cheng and Bi 2013), polymer composites, and straightforward conductors. Graphene oxide can be gained by the peeling of graphite oxide (Wu et al. 2013). The tunable oxygen and practical gatherings of graphene oxide encourage surface solutions and make it a promising material for the readiness of composites with natural and in natural materials.

Various modern advances are needed for hard water treatment process, which in numerous examples include a calcium evacuation stage (Zhao et al. 2015). Current ocean water handling innovations, for example, particle trade recuperation of magnesium, likewise oblige preparatory evacuation of calcium illustration is a preparatory treatment of ocean water preceding its further desalination. Profound calcination would tackle the issues of gypsum center arrange on radiator surfaces of distiller and stopping up of films in opposite osmosis or electrodialysis devices (Jiang et al. 2015).

This paper focus on synthesis, characterization and study the adsorption of calcium ions on the newly oxidized

مدينة الملك عبدالعزيز
للعلوم والتقنية KACST

🙟 Springer

graphene sheets from hard synthetic water, and also study the dynamic behavior of adsorption process by kinetic and isothermal models.

Experimental

Instrumentation

XRD characterization was performed on an X-ray Diffractometer System (D/MAX 2200H, Bede 200, Riga goes Instruments C). The FTIR spectrum (1000–2000 cm^{-1}) was measured using a Thermoscientific FTIR spectrometer with pure KBr as the background. The samples were mixed with KBr and the mixture was dried and compressed into a transparent tablet for measurement. The surface morphology of all the samples was analyzed using a high-resolution transmission electron microscope (HR-TEM, FEI Titan 80-300).

Preparation of cobalt silicate nanoparticles

Cobalt silicate nanoparticles were prepared according to (Fu et al. 2006). In this respect, 4.0 g of the freshly prepared cobalt nitrate and silica was vigorously stirred with 200 ml of ethanol for 30 min at 45 °C, then 40 ml of water, and 4 ml (1.4 M) of NaOH was added to the above suspension. Then the powder was separated and dried at 50 °C for 8 h in a vacuum oven.

Preparation of cobalt silicate nanoparticles

A cobalt silicate nanoparticle was prepared according to Stöber et al. method. In this respect, 4.0 g of the freshly prepared cobalt nitrate and silica were vigorously stirred with 200 ml of ethanol for 30 min at 45 °C, then 40 ml water, and 4 ml (1.4 M) NaOH was added to the above suspension. Then the powder was separated and dried at 50 °C for 8 h in a vacuum oven to get cobalt silicate nanoparticles (Calderón-Villajos et al. 2010; Wang et al. 2015a, b).

Rice straw pretreatments

The hemicellulose in rice straw was solubilized by dilute acid hydrolysis at 120 °C for 60 min, using 1 % (wt/wt) sulphuric acid. The resulting residue was subjected to the delignification process at 120 °C for 60 min using a mixture of 1.5 % (wt/wt) NaOH and 0.5 % (wt/wt) H$_2$O$_2$. During the dilute acid hydrolysis, the hemicellulose got solubilized in the form of monomeric sugars into the hydrolyzate and the succeeding delignification process removed lignin and a few amount of silica present in the pretreated rice straw into the black liquor.

Chemical exfoliation of cellulose

5 grams of cellulose were added to 5 ml of concentrated sulfuric acid in the presence of 0.1 g of silica and steered for 10 min., then filtrated and washing it with hot water until pH 7 and saved in an oven at 40 °C for 6 h. The prepared carbon material was poured in a flask in the presence of 0.01 g cobalt silicate nanoparticle and heated to 40 °C for 30 min. The prepared carbon nanomaterials were left to cool for 1 h, later dried in a vacuum oven for 24 h at 50–70 °C to obtain on graphene sheets (El-Sayed et al 2016).

Adsorption kinetics

The adsorption of kinetics studies was carried out on the freshly prepared Go in a 500 ml round bottom flask fitted with 500 mg/l of calcium ion concentration at pH 6. The solution is kept under continuous agitation with a magnetic stirrer at 600 RPM for 2 h, the sample was taken out for each 10 min and filtrated quickly on Whatman paper number GF-A layer, and the residual calcium ion concentration in the liquid phase was analyzed using AAS (Ma et al. 2009; Couper et al. 2012).

Adsorption isotherm

The adsorption isotherm studies are carried out for each 5 ml of fresh Go sheets in 50 ml round bottom flask fitted with 100, 200, and 500 mg/l calcium ion concentrations adjusted at pH 6, the temperature is varied between 20, 40, and 60 °C. The solution is kept under continuous agitation with a magnetic stirrer at 600 rpm for 2 h (Van de Steene et al. 2012; De Clercq et al. 2012). The sample was taken out for each 10 min and filtrated quickly on Whatman paper number GF-A layer. Then the calcium ion concentration was measured in the filtrates using AAS.

Results

FTIR analysis

The infrared spectra shown in Fig. 1 confirm absorption band observed at 2784 cm^{-1} is due to the C–H stretching of aromatic olefins (Fiocco et al. 2015). A strong, broad absorbance band observed at 3500 cm^{-1}, due to O–H stretching vibrations. The spectra exhibit a broad between 2500 and 3800 cm^{-1}, corresponding to the stretching vibrations band of the surface silanols Si–OH perturbed

Fig. 1 FTIR of silica nanoparticles
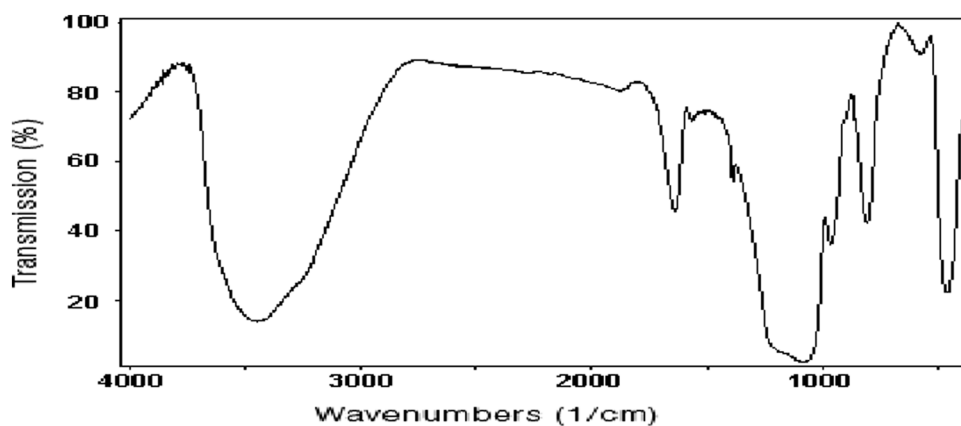
Fig. 2 FTIR of microcrystalline cellulose
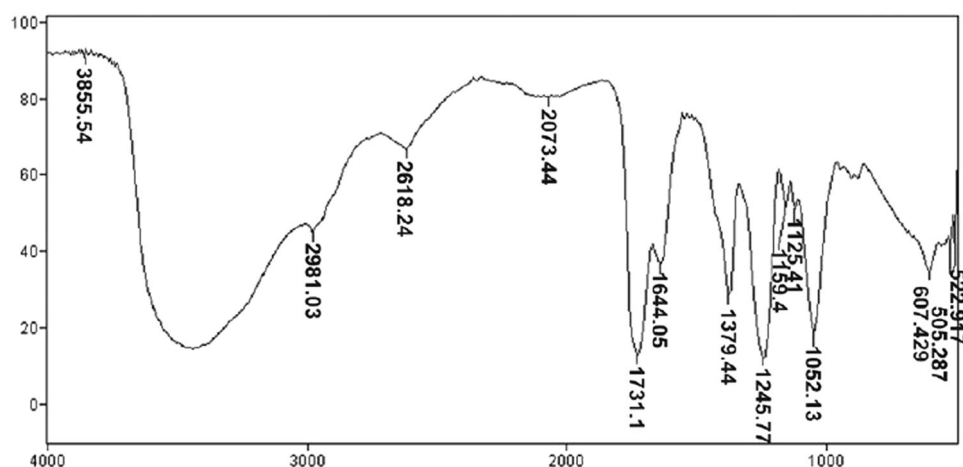
either by hydrogen bonding intramolecularly or with adsorbed water. Below 1500 cm^{-1}, the spectra exhibit a broad and intense band around 1100 cm^{-1}, characteristic of the ant symmetric stretching vibration of the Si–O–Si, thoroughly drying the sample before analysis will cut out vibrations due to water, while surface –OH groups can be significant and a less intense band around 900 cm^{-1} (Si–O–Si asymmetric stretching vibrations). A weaker O–H bending vibration band is seen at 1600 cm^{-1}. Both adsorbed water and surface –OH groups contribute to these bands.

Figure 2 shows the IR-spectrum of white microcrystalline cellulose from 800 to 2000 cm^{-1}. The absorption bands at 1593, 1408, and 1317 cm^{-1} are assigned to asymmetrical COO– stretching, symmetrical stretching and C–H bending, respectively. The appearance of these bands confirms the formation of microcrystalline cellulose (Zhao et al. 2011; Bettaieb et al. 2015; Chen et al. 2015a, b). The infrared spectra shown in Fig. 2 confirm an absorption band observed at 2901 cm^{-1} this is due to the C–H vibration stretch of the –CH$_2$ groups from primary alcohols. The other band of interest is observed at

2000–2100 cm^{-1}, where a comparison of the two spectra reveals modifications, with emphasis on the band at 1750 cm^{-1}, which is attributed to the axial deformation vibration of C=O from carboxylic acids.

The FT-IR spectra of GO in Fig. 3 that was shows the presence of various oxygen functional groups in GO appeared as a broadband at 3000–3700 cm^{-1} was contributed to hydroxyl groups, due to the water molecules and to the hydroxyl groups of GO. A band at 1760 cm^{-1} was assigned to be the C–O stretching vibrations of the COOH groups and the band at 1600 cm^{-1} would be considered to be the vibration of C (Aleksandrzak et al. 2015). A weak peak located at 1350 cm^{-1} was assigned to be the OH bending of the C–OH groups (Bavand et al. 2015). A strong band at 1100 cm^{-1} might be attributed to C–O stretching vibration (Chang et al. 2015; Singh et al. 2015).

Raman analysis

Raman spectra can be divided into two regions. The region below 1600 cm^{-1} (especially below 700 cm^{-1}) is most sensitive to the conformation of the cellulose backbone, but
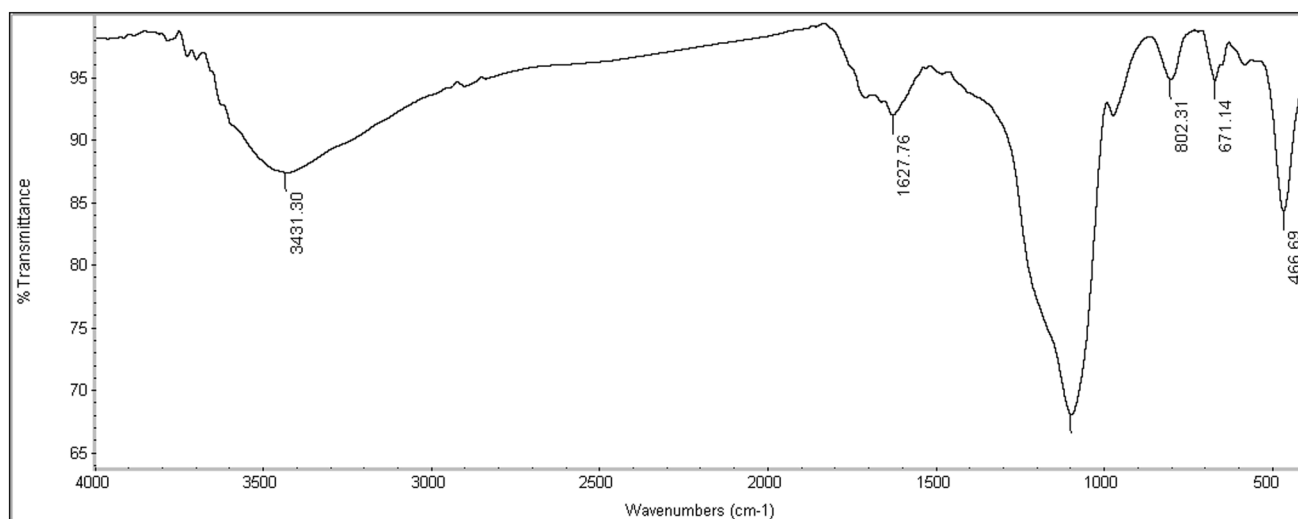
Fig. 3 FTIR of graphene oxide sheets result from cellulose powder
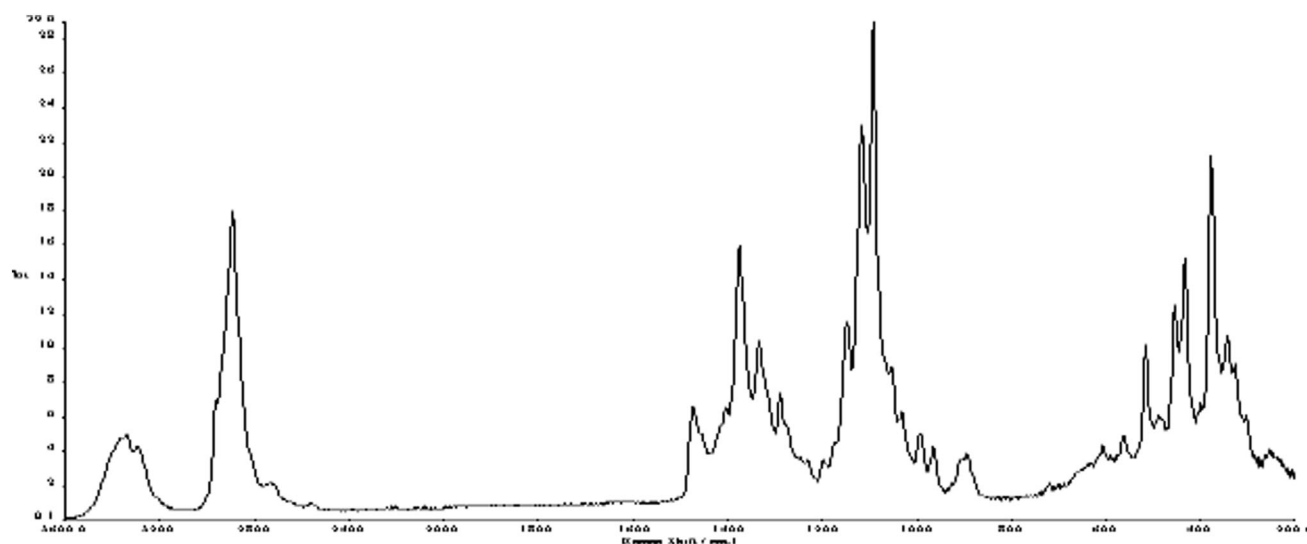

Fig. 4 Raman spectroscopy of microcrystalline cellulose

the region above 2700 cm^{-1} is more sensitive to hydrogen bonding (Altava et al. 2001; Chen et al. 2015a, b). Figure 4 presents Raman spectra of cellulose I for the 150–1650 cm^{-1} spectral range. The spectra are for microcrystalline celluloses (cellulose powder, Aldrich) from rice straw as an example of different proportions of crystalline cellulose. This would suggest that microcrystalline cellulose contains a higher crystalline cellulose (Ribeiro-Soares et al. 2015).

Raman spectroscopy is the most appealing technique to characterize carbon compounds because of its nondestructive, fast and high-resolution analysis, and gives the structural and electronic information as shown in Fig. 5 (Chang et al. 2015). All the sp^2 carbon materials exhibit a

very sharp peak around 2500–2800 cm^{-1} in the Raman spectra (Chen et al. 2015a, b). A sharp 2D-band around 2690–2700 cm^{-1} in is a signature of the sp^2 graphitic system. The 2D-band is a second-order two-phonon process and frequency dependent on the energy of excitation laser (Tiwari et al. 2015).

So, it can be used to quantify the number of graphene layers. The shape and nature of 2D band are pretty much different from that in the single-layered and few-layered graphene (Giusca et al. 2015) is due to E_{2g} mode at the Γ-point and it arises from the stretching mode of C–C bond in graphitic materials, and is common to all sp^2 carbons.

It is highly sensitive to strain effects in the sp^2 system; thus, the D-band represents the disordered structure of
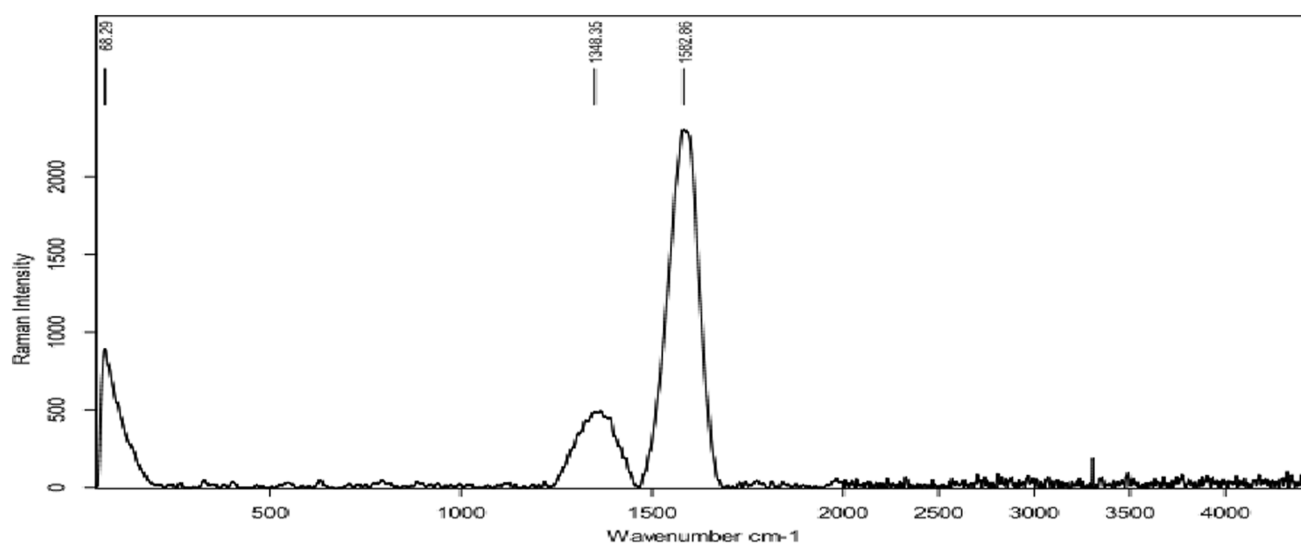
**Fig. 5** Raman spectroscopy of graphene oxide sheets
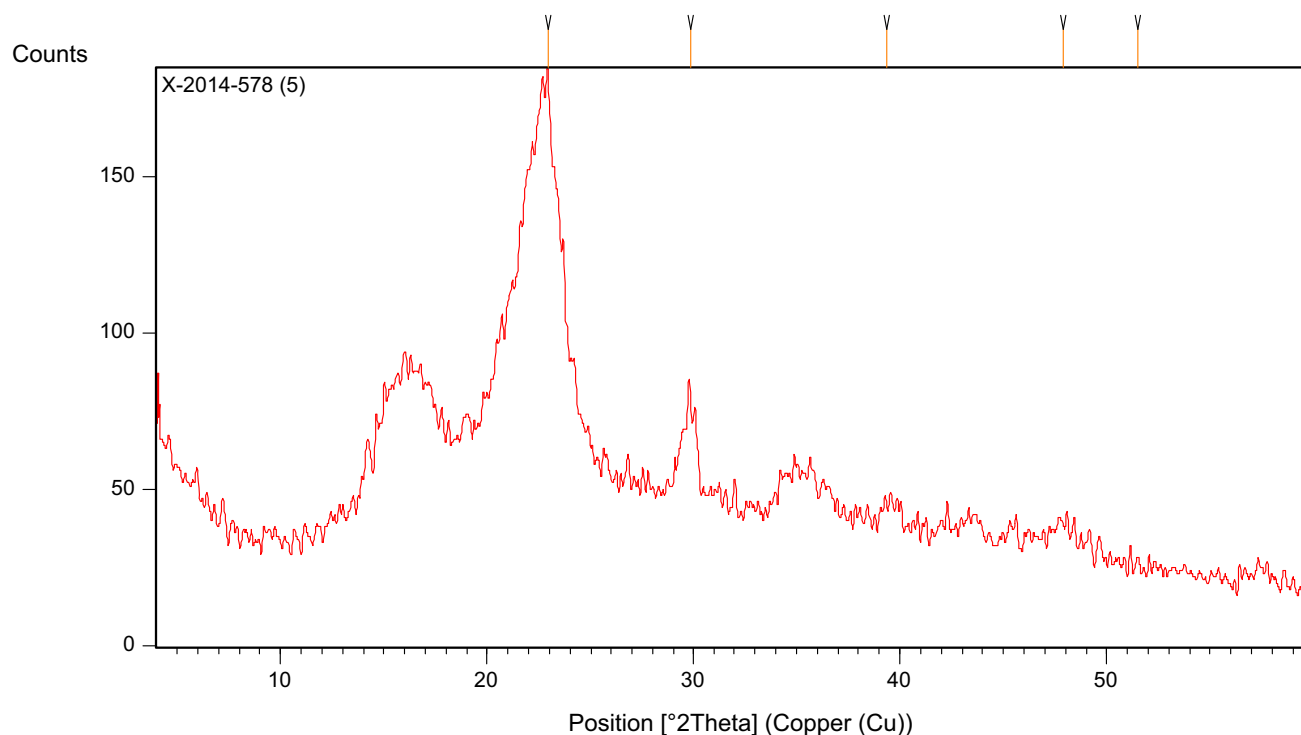
Fig. 6 XRD of cellulose powder

graphene (mainly sp^3 hybridized carbon atoms) which makes Raman spectroscopy as one of the most sensitive techniques to characterize graphene and its derivatives. The typical feature of graphene can be characterized by G-band at ~ 1580 cm^{-1}, and 2D band at ~ 2710 cm^{-1} appears for GO samples. GO sample shows prominent D-band peak at ~ 1350 cm^{-1}. Other defective bands such as D band (1620 cm^{-1}) and D + G band (2947 cm^{-1}) are absent in GO samples (Singh et al. 2015).

X-ray analysis

Figure 6 shows the XRD pattern of the microcrystalline cellulose. The cellulose displays a broad diffraction with 2θ ranging from 5° to 35°, suggesting the amorphous structure of the polymeric scaffold (Oun and Rhim 2015). Besides the broad diffraction ascribed to the polymeric scaffold, the diffraction pattern for pristine MCC shows an intense peak at 15°, 16°, 22°, 23° and 26° that are the characteristic
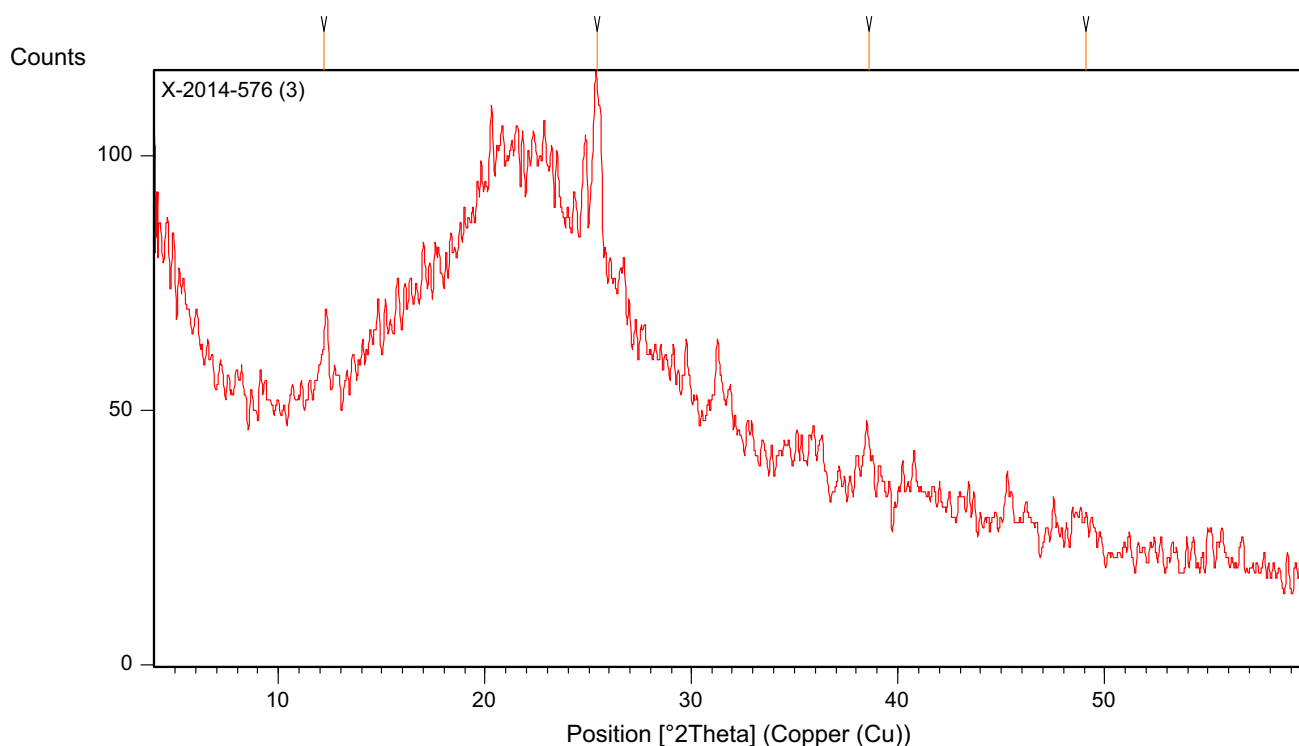
Fig. 7 XRD of graphene sheets from microcrystalline cellulose

peaks of microcrystalline cellulose fibers, which coincides with reported literature values (Lopes et al. 2015; Ribeiro-Soares et al. 2015).

Figure 7 presents the XRD patterns of GO. The d spacing of the lowest peak is found to be 1.0–1.02 nm, which is 20 % larger than that of pristine GO (Giri et al. 2013; Modak et al. 2015. We found that GO exhibited two—$\approx 12.9°$ and $22.7°$. The former peak is correlated to an interlayer spacing of 0.68 nm in the layer-like GO. This value can be assigned to the (001) reflection peak and might depend on the method of preparation and on the number of layers of water in the gallery space of GO at $2\theta \approx 22.7°$ relative to (002) plane (Giusca et al. 2015).

Thermal analysis

Thermal gravity analysis (TGA) was carried out on the synthesized microcrystalline cellulose fibers, and the result is presented in Fig. 8. Two distinct weight losses are observed in the thermogram of MCC fibers. The first weight loss is about 24.51 % and started at temperature range between 30 and 135 °C, this may be due to the moisture in the sample. This is because biopolymer absorbs moisture from its surroundings as reported by Oun and Rhim (2015). A similar observation has been reported by Quinlan et al. (2015). The second weight loss is 14.79 % and started at temperature range of 250–323 °C due to the

loss of COO– from the polysaccharide, our assumption are in a good agrement with that found by Shen et al. (2014). The final loss is about 7.05 % and observed at temperature range between 373 and 511 °C, representing the degradation of the remaining material into carbon residues.

The thermogravimetric analysis results showed that the graphene sheets had good thermal stability below 400 °C and up to 600 °C. The mass loss at a temperature below 100 °C is due to the removal of absorbed water and can be seen for all samples in Fig. 9. For GO, two stages of mass loss are shown; the first stage starts at 150 °C is due to the loss of hydroxyl, epoxy functional groups and remaining water molecules. The second stage lay between 450 and 650 °C and involved the pyrolysis of the remaining oxygen-containing groups and cause formation of carbon ring (Dong et al. 2015). Finally, a slight weight loss appeared from 250 to 800 °C is caused by the decomposition of the carbon skeleton.

HR-TEM analysis

HR-TEM analyses in Fig. 10 showed that the cobalt silicate nanoparticles got by co-precipitation and hydrothermal processes could be readily tailored by varying reaction time, this due to high respect ratio, high surface area, high reactivity, agglomeration and aggregation of cobalt silicate nanoparticles, and the possibility of creating a new material with peculiar properties.

Fig. 8 TGA of cellulose powder
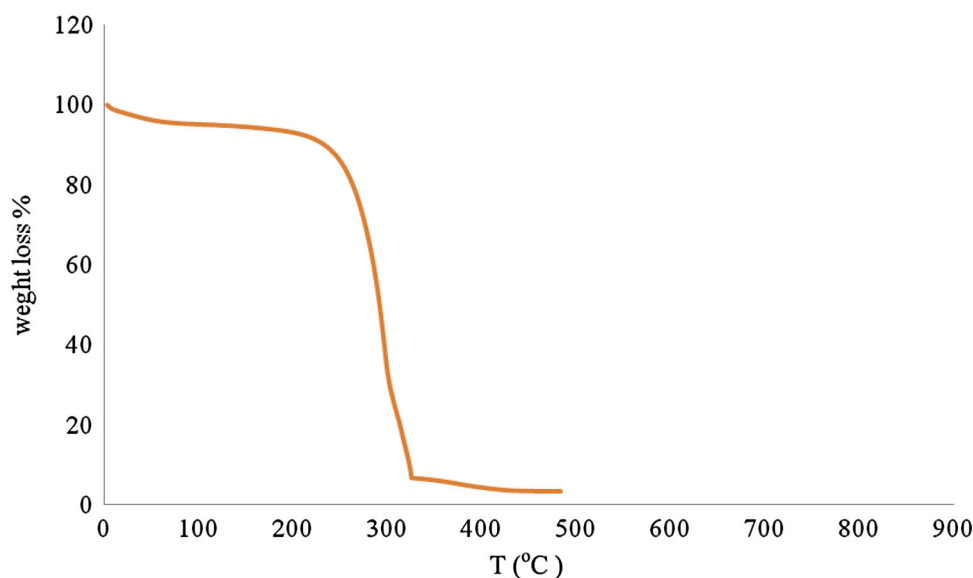
Fig. 9 TGA of graphene oxide sheets
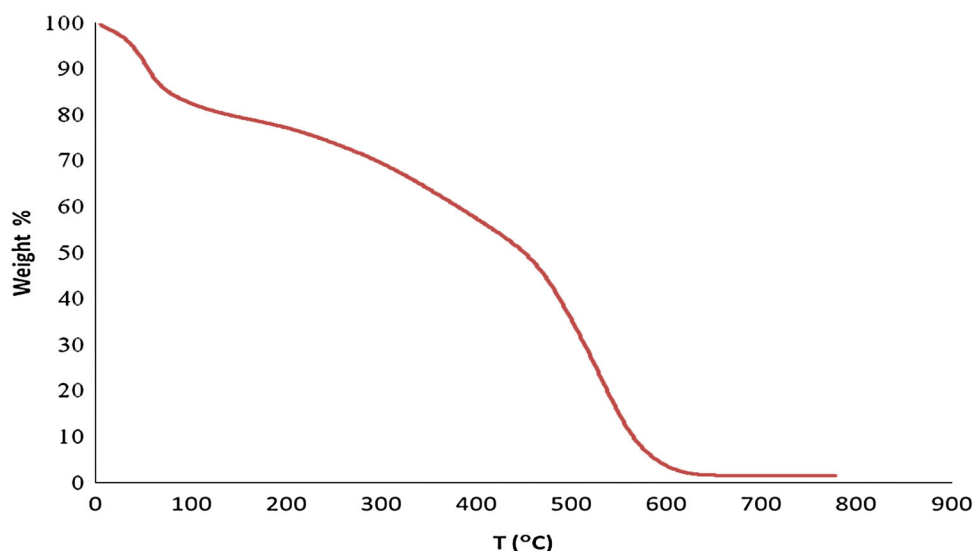
HR-TEM micrograph of a very dilute suspension cellulose nanoparticles in Fig. 11, showing agglomerated fiber network. The diameter of cellulose fiber has a wide range of distribution, but the size lies within the range of the most 'network-like' and their length lay between 250 and 480 nm and their diameter between 20 and 60 nm. Their compact agglomeration of cellulose nanoparticles shows that cellulose chains have an intermolecular hydrogen bonding and a strong hydrophilic interaction in between the cellulosic chains (Trache et al. 2014).

The heterostructure of graphene sheets are verified by morphological analyzer of SEM, HR-TEM and SAED images. HR-TEM of graphene sheets in Fig. 12 show that transparent carbon sheets almost have diameters achieved between 40 and 200 nm. This means that the cobalt silicate nanoparticles on the graphene surface acted as nanoscale spacers and increases the spacing between the next carbons sheets, thereby, preventing van der Waals contacts between neighboring graphene sheets and a corresponding graphitic structure. We found that the anchored cobalt silicate nanoparticles distributed uniformly on these single carbon sheet. These monolayer sheets have a large area, therefore, their particles can deposit on both sides of these sheets and make an excellent candidates for the electrochemical application (Dong et al. 2015).
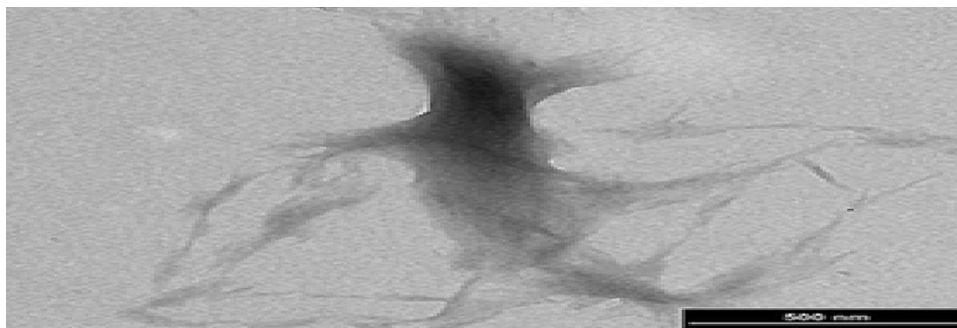
SAED analysis

The absence of diffuse diffraction ring pattern and presence of spot pattern in SAED image in Fig. 13, confirmed the crystalline graphitic layer of the prepared graphene oxide sheets as illustrated by Giri et al. (2013). The mechanism
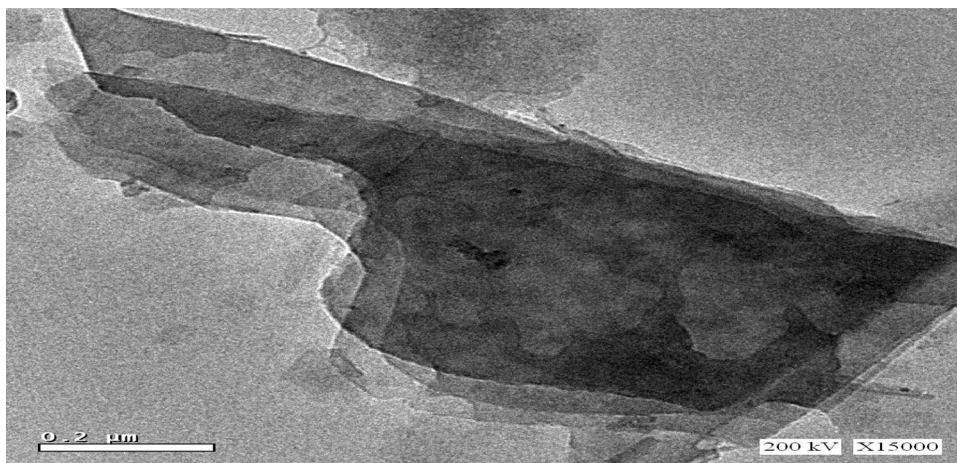
Fig. 10 HR-TEM of cobalt silicate nanoparticles
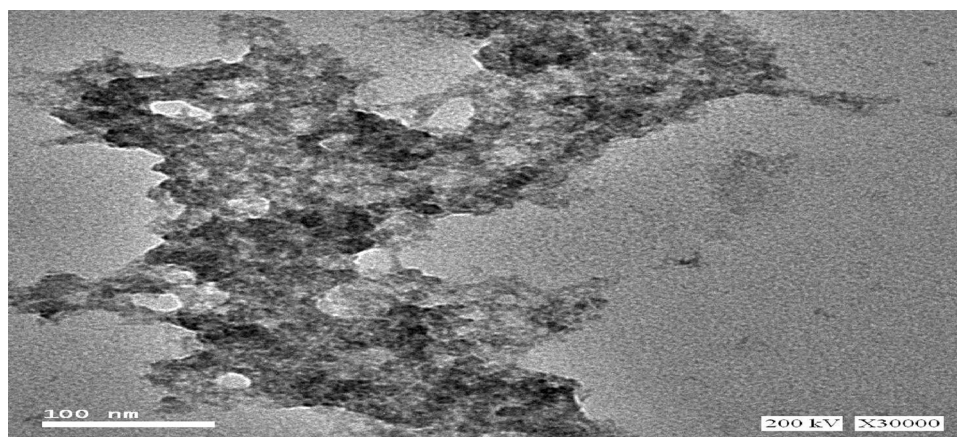
Fig. 11 HR-TEM of cellulose powder

Fig. 12 HR-TEM of graphene sheets

and efficiency of exfoliation can be explained based on cobalt silicates nanoparticles intercalation and exfoliation of graphene sheets during the chemical process as explained in the mechanism of exfoliation section.

Effect of contact time and adsorption kinetics

To show contact time between the oxides graphene sheets and calcium ion solution, the adsorption capacities of calcium ion were measured as a function of time as illustrated in Fig. 14. The plot shows that the rate of Ca(II) adsorption is higher at the beginning time until 60 min., because the bigger surface territory of the oxide graphene sheets being accessible at starting for the adsorption of calcium ions (Zhao et al. 2011).

As the surface of the adsorption process appears to get to be depleted, the uptake rate is controlled by the rate at which the adsorbent is transported from the outside to the inside locales of the adsorbent particles. The rate of Ca(II) evacuation achieved roughly after 60 min blending. It does

Fig. 13 SAED of graphene
sheets
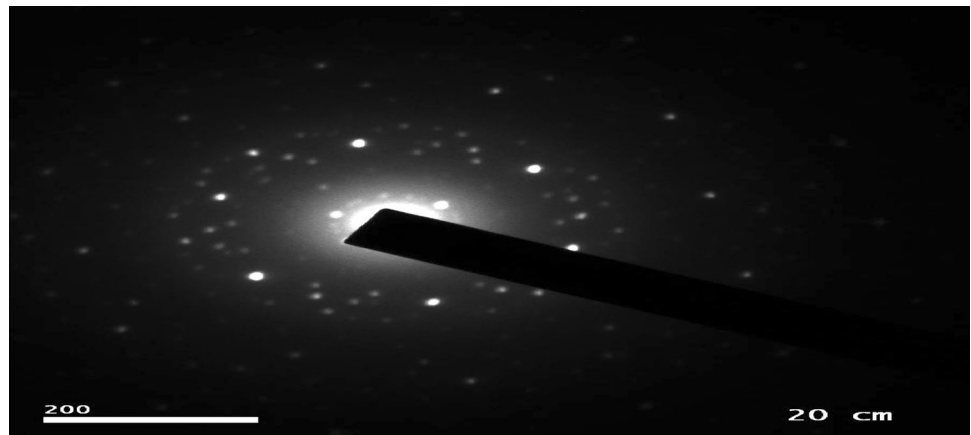
Fig. 14 Contact time study of
calcium ions adsorption on
graphene sheets
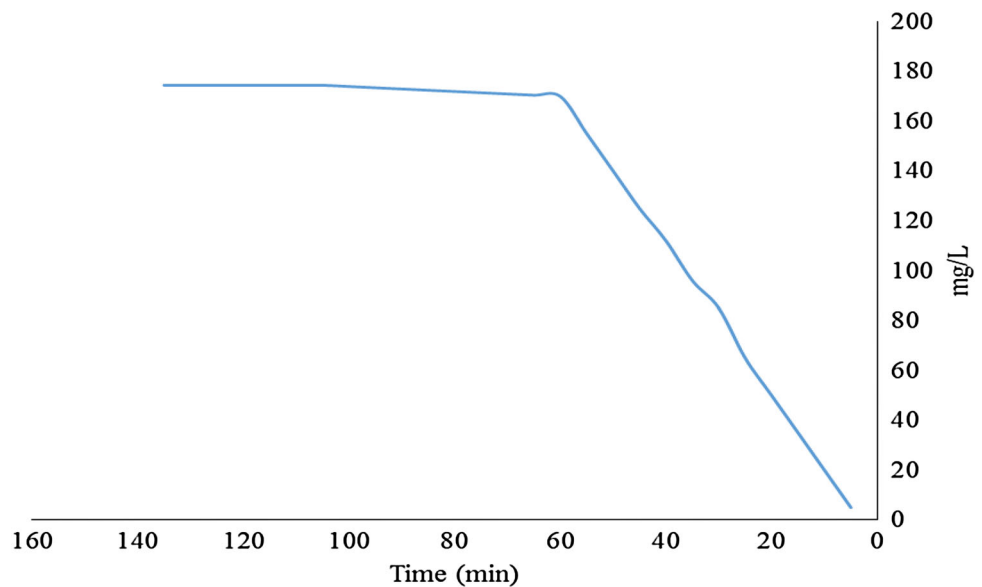
not appear to enjoy much a blending time longer than 2 h
as like other works (Agarwal et al. 2016; Ahmed and Jhung
2016). Then along these lines, balance time of 60 min, was
chosen for each single further study.

The kinetic equations were developed to explain the
transport of calcium ions onto adsorbents as illustrated in
Figs. 15 and 16). These equations include the pseudo-first-
order equation, the pseudo-second-order equation, and
second-order rate equation model (Baláž et al. 2015; Liu
et al. 2016a, b).

The pseudo-first-orders was given by:

$$\log(q_e - q) = \log q_e - \frac{k_{1,ads}t}{2.303},$$

where w_e (constant of pseudo-first-order adsorption
(min^{-1}). $k_{1,ads}$, and q_e can be determined from slope and
intercept, respectively (Liu et al. 2015a, b).

The pseudo-second-order reaction kinetic is expressed
as:

$$\frac{t}{q} = \frac{1}{k_{2,abs}q_e^2} + \frac{t}{q_t},$$

where $k_{2,abs}$ is the rate constant of pseudo-second-order
absorption (g/(again)) and q_e is the adsorption capacity at
equilibrium (mg/g).

The second-order rate equation is expressed as

$$\frac{1}{(q_e - q_t)} = \frac{1}{q_e} + k^0 t,$$

where q_e and q_t are the amounts of metal ion sorbed at
equilibrium and at any time (mg/g), respectively, but k^0 is
second-order rate constant of adsorption (g/(mg min)) (Liu
et al. 2015a, b).

As shown from the kinetic parameters in Table 1 The
correlation coefficients of pseudo-first-order kinetic less
than 0.99, whereas the correlation coefficients of the sec-
ond-order are more noteworthy than 0.99 and that gives the
best association of data to apply for the second order

Fig. 15 The pseudo-first-orders of calcium ion adsorption on oxidized graphene sheets
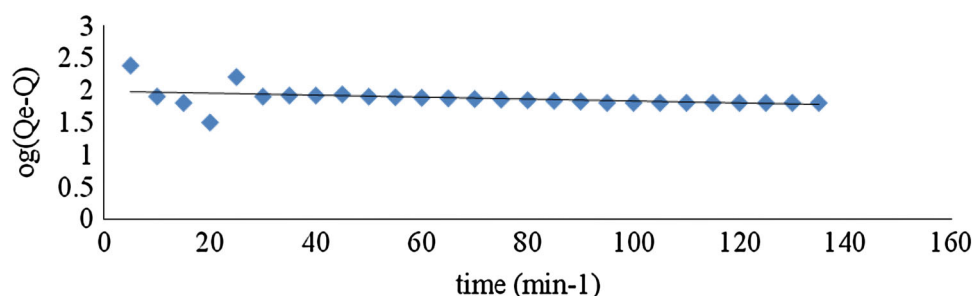
Fig. 16 Pseudo-second-order adsorption of calcium ion adsorption on graphene sheets
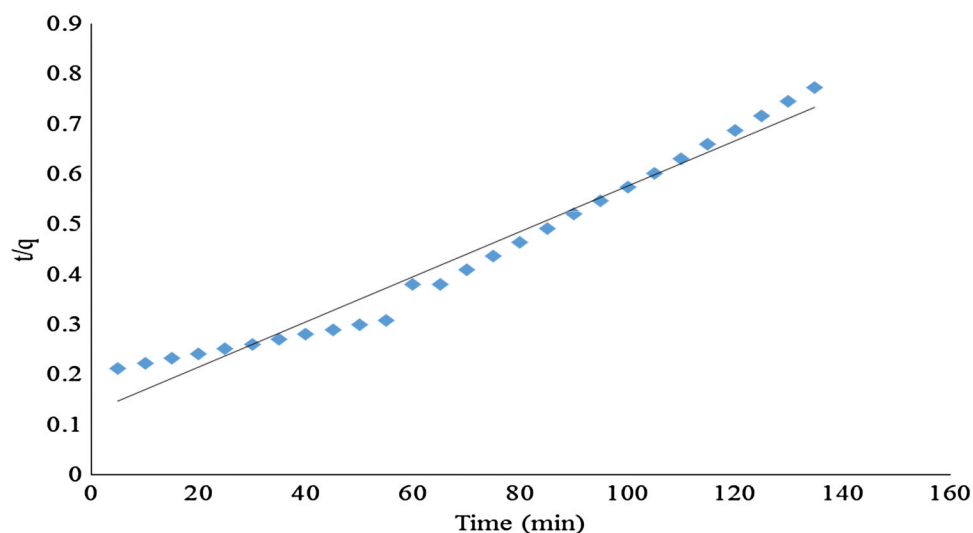
Table 1 Adsorption kinetic parameters of calcium ions on oxidized graphene sheets

Pseudo-first-order kinetic model			Pseudo-second-order kinetic model		
k_{pf} (min^{-1})	q_e (mg/g)	R^2	k_{ps} (g/(mg min))	q_e (mg/g)	R^2
0.001	1.980	0.174	0.005	0.030	0.997

adsorption model of Ca(II) onto oxidized graphene sheets. We found that, adsorption kinetic parameters of calcium ion on our oxidized graphene sheets agree with the adsorption nature of the other graphene oxide. Which is produced by another process with increasing adsorption capacity of our graphene oxidized sheets toward calcium ions respecting to other ions in the same rank, so a pseudo-second demand model can be considered (Pang et al. 2016, Liu et al. 2016a, b; Tan et al. 2016). The latter is shown that the rate determining step may be chemical adsorption one through the exchange of electrons amidst adsorbent and adsorbate.

Effect of temperatures variations

The effect of temperature of ions sorption on GO is represented in Fig. 17. Over the investigated temperature range (298–345 K) (Gogoi and Dutta 2016), it is clear that

the maximal removal occur at higher temperature, i.e., the temperature-give up effect appear to be particularly pronounced. The removal of calcium ions by Go has been shown to be greatest at 340 K. We found that the high temperatures could not affect active sites and uptake of ions, also leading to the increase of uptake levels (Jiang et al. 2016).

Equilibrium isotherm

Equilibrium isotherm equations are used to describe experimental sorption data. The equation parameters and the underlying thermodynamic assumptions of these equilibrium models often provide some insight into both the sorption mechanism, the surface properties and affinity of the sorbent (Liu et al.; Acar et al. 2015). Langmuir isotherm can be characterized by a plateau graphically. The saturation point reaches an equilibrium where no further

Fig. 17 Effect of temperature on Go removal for adsorption of Ca^{+2}
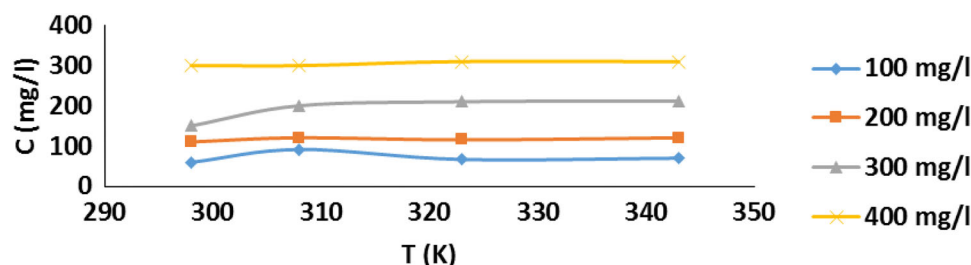
Table 2 Adsorption constants of the adsorption of Ca(II) on oxidized graphene sheets at temperature 35 °C

Freundlich constant			Langmuir constant			
K	n	R^2	q_e	q^0	b	R^2
0.729	0.609	0.9950	190	500	0.668	0.107

adsorption occurs. Adsorption is assumed to take place at specific homogeneous sites within the adsorbent (Xin et al. 2015). Once a sorbate molecule occupies a site, northern adsorption takes place at that site. A linearized form of Langmuir model is:

$$\frac{C_e}{q_e} = \frac{1}{X_m K_L} + \frac{C_e}{X_m},$$

where, K_L (dm^3/g) is Langmuir constant termed as the apparent energy of adsorption and X_m (mg/g) is sorption capacity.

freundlich empirical models contributed to non-ideal sorption on heterogeneous surfaces and multilayer sorption and is expressed by the following equation:

$$\log q_e = \frac{1}{n} \log C_e + \log k,$$

where, 1/n and k are Freundlich constants. The Freundlich isotherm parameter 1/n measures the absorption intensity of metal ions on prepared resins and Freundlich constant k is the adsorption capacity of prepared graphene sheets.

It demonstrates that the adsorption of Ca(II) onto oxidized graphene sheets is not a monolayer sort, one that does not completely inlet the surface of the oxidized graphene sheets. As seen from Table 2, Langmuir isotherm not fits well with the trial information. This may be because of the heterogeneous appropriation of dynamic destinations on the oxidized graphene sheets. Regarding the Freundlich model, the plots of log C_e versus log C_e at different temperatures were found to be directly sowing the tangibility of the Freundlich model. The catch of the line is pretty nearly a marker as far as possible, and the inclination indicates adsorption force. The Freundlich parameters and the results are addressed in Table 2. It is probably comprehended that the Langmuir isotherm contrasts with an overwhelming molecule exchange part while the Freundlich isotherm shows adsorption-complexion reactions happening in the adsorption process.

Conclusion

The accompanying conclusions can be taken into account the examination of calcium ions adsorption on the evacuated graphene oxidized sheets.

The modelling of kinetic curves has also been investigated. It is found that the best fit was achieved with the pseudo-second-order model mechanism. However, the data did not fit the pseudo-first-order model, which indicates the likelihood of a chemical adsorption mechanism.

Besides, the adsorption of calcium ions under varied temperature and contact time parameters. Temperature variation studies have shown an endothermic process and the percentage removal of both metal ions have increases with temperature.

Both Langmuir and Freundlich isotherms have been used to display the isothermal adsorption process of Ca(II) on oxidized graphene sheets. It is found that the Freundlich is the acceptable model for adsorption of specific calcium ions on oxidized graphene sheets, i.e., the un-uniform surface of graphene sheets having a heterogeneous active site on its surface.

Else, oxidized graphene sheets show an impression of being a good adsorbent for the calcium ions from the underground hard water. At these adsorption levels of graphene oxide sheets, a packed column method using oxidized graphene sheets for the removal of calcium ions is possibly more effective than current strategic advancement like Ro.

References

Acar ET, Ortaboy S, Atun G (2015) Adsorptive removal of thiazine dyes from aqueous solutions by oil shale and its oil processing residues: characterization, equilibrium, kinetics and modeling studies. Chem Eng J 276:340–348

Agarwal S, Tyagi I, Gupta VK, Bagheri AR, Ghaedi M, Asfaram A, Hajati S, Bazrafshan AA (2016) Rapid adsorption of ternary dye pollutants onto copper (I) oxide nanoparticle loaded on activated carbon: experimental optimization via response surface methodology. J Environ Chem Eng 4(2):1769–1779

Ahmed I, Jhung SH (2016) Adsorptive desulfurization and denitrogenation using metal-organic frameworks. J Hazard Mater 301:259–276

Aleksandrzak M, Adamski P, Kukułka W, Zielinska B, Mijowska E (2015) Effect of graphene thickness on photocatalytic activity of TiO_2-graphene nanocomposites. Appl Surf Sci 331:193–199

Altava B, Burguete MI, García-Verdugo E, Luis SV, Vicent MJ (2001) The use of NIR-FT-Raman spectroscopy for the characterization of polymer-supported reagents and catalysts. Tetrahedron 57(41):8675–8683

Baláž M, Bujňáková Z, Baláž P, Zorkovská A, Danková Z, Briančin J (2015) Adsorption of cadmium(II) on waste biomaterial. J Colloid Interface Sci 454:121–133

Bavand R, Yelon A, Sacher E (2015) X-ray photoelectron spectroscopic and morphologic studies of Ru nanoparticles deposited onto highly oriented pyrolytic graphite. Appl Surf Sci 355:279–289

Bettaieb F, Khiari R, Dufresne A, Mhenni MF, Belgacem MN (2015) Mechanical and thermal properties of *Posidonia oceanica* cellulose nanocrystal reinforced polymer. Carbohydr Polym 123:99–104

Calderón-Villajos R, Zaldo C, Cascales C (2010) Hydrothermal processes for Tm3+-doped GdV O4 nanocrystalline morphologies and their photoluminescence properties. Phys Proc 8:109–113

Chang Y-N, Ou X-M, Zeng G-M, Gong J-L, Deng C-H, Jiang Y, Liang J, Yuan G-Q, Liu H-Y, He X (2015) Synthesis of magnetic graphene oxide–TiO_2 and their antibacterial properties under solar irradiation. Appl Surf Sci 343:1–10

Chen J, Shi X, Qi S, Mohai M, Bertóti I, Gao Y, Dong H (2015a) Reducing and multiple-element doping of graphene oxide using active screen plasma treatments. Carbon 95:338–346

Chen W, Li Q, Cao J, Liu Y, Li J, Zhang J, Luo S, Yu H (2015b) Revealing the structures of cellulose nanofiber bundles obtained by mechanical nanofibrillation via TEM observation. Carbohydr Polym 117:950–956

Cheng X, Bi XT (2013) Modeling and simulation of nitrogen oxides adsorption in fluidized bed reactors. Chem Eng Sci 96:42–54

Couper JR, Penney WR, Fair JR, Walas SM (2012) 15—Adsorption and ion exchange. Chemical process equipment, 3rd edn. Butterworth-Heinemann, Boston, pp 529–559

De Clercq N, Moens K, Depypere F, Dewettinck k (2012) Influence of cocoa butter refining on the quality of milk chocolate. J Food Eng 111(2):412–419. doi:10.1016/j.jfoodeng.2012.01.033

Dong Y, Yung KC, Ma R, Yang X, Chui Y-S, Lee J-M, Zapien JA (2015) Graphene/acid assisted facile synthesis of structure-tuned Fe_3O_4 and graphene composites as anode materials for lithium ion batteries. Carbon 86:310–317

El-Sayed M, Ramzi M, Hosny R, Fathy M, Abdel Moghny Th (2016) Breakthrough curves of oil adsorption on novel amorphous carbon thin film. Water Sci Technol 73(10):2361–2369. doi:10.2166/wst.2016.072

Fiocco L, Elsayed H, Daguano JKMF, Soares VO, Bernardo E (2015) Silicone resins mixed with active oxide fillers and Ca–Mg Silicate glass as alternative/integrative precursors for wollastonite–diopside glass-ceramic foams. J Non-Cryst Solids 416:44–49

Fu Q, Johanson CM, Wallace JM, Reichler T (2006) Enhanced mid-latitude tropospheric warming in satellite measurements. Science 312(5777):1179. doi:10.1126/science.1125566

Giri S, Ghosh D, Das CK (2013) In situ synthesis of cobalt doped polyaniline modified graphene composites for high performance supercapacitor electrode materials. J Electroanal Chem 697:32–45

Giusca CE, Perrozzi F, Melios C, Ottaviano L, Treossi E, Palermo V, Kazakova O (2015) Electrostatic transparency of graphene oxide sheets. Carbon 86:188–196

Gogoi S, Dutta RK (2016) Fluoride removal by hydrothermally modified limestone powder using phosphoric acid. J Environl Chem Eng 4(1):1040–1049

Jiang T, Liu W, Mao Y, Zhang L, Cheng J, Gong M, Zhao H, Dai L, Zhang S, Zhao Q (2015) Adsorption behavior of copper ions from aqueous solution onto graphene oxide–CdS composite. Chem Eng J 259:603–610

Jiang L, Nelson GW, Han SO, Kim H, Sim IN, Foord JS (2016) Natural cellulose materials for supercapacitors. Electrochim Acta 192:251–258

Lin Z, Waller GH, Liu Y, Liu M, Wong C-P (2013) 3D Nitrogen-doped graphene prepared by pyrolysis of graphene oxide with polypyrrole for electrocatalysis of oxygen reduction reaction. Nano Energy 2(2):241–248

Liu J, Cao J, Chen H, Zhou D (2015a) Adsorptive removal of humic acid from aqueous solution by micro- and mesoporous covalent triazine-based framework. Colloids Surf A: Physicochem Eng Asp 481:276–282

Liu W, Zhang J, Jin Y, Zhao X, Cai Z (2015b) Adsorption of Pb(II), Cd(II) and Zn(II) by extracellular polymeric substances extracted from aerobic granular sludge: efficiency of protein. J Environ Chem Eng 3(2):1223–1232

Liu Q, Liu Q, Ruan Z, Chang X, Yao J (2016a) Removal of Cu(II) from aqueous solution using synthetic poly(catechol-diethylenetriamine-*p*-phenylenediamine) particles. Ecotoxicol Environ Saf 129:273–281

Liu W, Zhao X, Wang T, Zhao D, Ni J (2016b) Adsorption of U(VI) by multilayer titanate nanotubes: effects of inorganic cations, carbonate and natural organic matter. Chem Eng J 286:427–435

Lopes TR, Gonçalves GR, de Barcellos Jr E, Schettino MA Jr, Cunha AG, Emmerich FG, Freitas JCC (2015) Solid state 27Al NMR and X-ray diffraction study of alumina–carbon composites. Carbon 93:751–761

Ma F, Qu R, Sun C, Wang C, Ji C, Zhang Y, Yin P (2009) Adsorption behaviors of Hg(II) on chitosan functionalized by amino-terminated hyperbranched polyamidoamine polymers. J Hazard Mater 172(2–3):792–801

Modak P, Kondawar SB, Nandanwar DV (2015) Synthesis and characterization of conducting polyaniline/graphene nanocomposites for electromagnetic interference shielding. Proc Mater Sci 10:588–594

Oun AA, Rhim J-W (2015) Preparation and characterization of sodium carboxymethyl cellulose/cotton linter cellulose nanofibril composite films. Carbohydr Polym 127:101–109

Pang Z, Shi X, Wei Y, Fang D (2016) Grain boundary and curvature enhanced lithium adsorption on carbon. Carbon

Quinlan PJ, Tanvir A, Tam KC (2015) Application of the central composite design to study the flocculation of an anionic azo dye using quaternized cellulose nanofibrils. Carbohydr Polym 133:80–89

Ribeiro-Soares J, Oliveros ME, Garin C, David MV, Martins LGP, Almeida CA, Martins-Ferreira EH, Takai K, Enoki T, Magalhães-Paniago R, Malachias A, Jorio A, Archanjo BS, Achete CA, Cançado LG (2015) Structural analysis of polycrystalline graphene systems by Raman spectroscopy. Carbon 95:646–652

Shen S, Cai B, Wang C, Li H, Dai G, Qin H (2014) Preparation of a novel carbon-based solid acid from cocarbonized starch and polyvinyl chloride for cellulose hydrolysis. Appl Catal A 473:70–74

Singh K, Srivastava G, Talat M, Srivastava ON, Kayastha AM (2015) α-Amylase immobilization onto functionalized graphene nanosheets as scaffolds: its characterization, kinetics and potential applications in starch based industries. Biochem Biophys Rep 3:18–25

Tan L, Wang S, Du W, Hu T (2016) Effect of water chemistries on adsorption of Cs(I) onto graphene oxide investigated by batch and modeling techniques. Chem Eng J 292:92–97

Tiwari SK, Huczko A, Oraon R, De Adhikari A, Nayak GC (2015) Facile electrochemical synthesis of few layered graphene from discharged battery electrode and its application for energy storage. Arab J Chem

Trache D, Donnot A, Khimeche K, Benelmir R, Brosse N (2014) Physico-chemical properties and thermal stability of microcrystalline cellulose isolated from Alfa fibres. Carbohydr Polym 104:223–230

Van de Steene E, De Clercq J, Thybaut JW (2012) Adsorption and reaction in the transesterification of ethyl acetate with methanol on Lewatit K1221. J Mol Catal A: Chem 359:57–68

Wang X, Zhang L, Kuan P, Wang S, Yu C, Li K, Chen D, Hu L (2015a) Spectroscopy and 2 μm laser behaviors of Al3+/Ho3+ CO-doped silica fiber. Mater Lett 158:442–444

Wang Y, Wang X, Wang Y, Li J (2015b) Acid-treatment-assisted synthesis of Pt–Sn/graphene catalysts and their enhanced ethanol electro-catalytic activity. Int J Hydrog Energy 40(2):990–997

Wu S, Zhao X, Li Y, Zhao C, Du Q, Sun J, Wang Y, Peng X, Xia Y, Wang Z, Xia L (2013) Adsorption of ciprofloxacin onto biocomposite fibers of graphene oxide/calcium alginate. Chem Eng J 230:389–395

Xin Y, Bligh MW, Kinsela AS, Wang Y, David Waite T (2015) Calcium-mediated polysaccharide gel formation and breakage: impact on membrane foulant hydraulic properties. J Membr Sci 475:395–405

Zhao X, Song L, Fu J, Tang P, Liu F (2011) Adsorption characteristics of Ni(II) onto MA–DTPA/PVDF chelating membrane. J Hazard Mater 189(3):732–740

Zhao J, Li H, Liu Z, Hu W, Zhao C, Shi D (2015) An advanced electrocatalyst with exceptional eletrocatalytic activity via ultrafine Pt-based trimetallic nanoparticles on pristine graphene. Carbon 87:116–127